

Forecasting mortality rates with functional signatures

Yap Zhong Jing¹, Dharini Pathmanathan¹, and Sophie Dabo-Niang²

¹Institute of Mathematical Sciences, Faculty of Science, Universiti Malaya, 50603 Kuala Lumpur, Malaysia

²CNRS, UMR 8524-Laboratoire Paul Painlevé, INRIA-MODAL, Université Lille, F-59000 Lille, France

July 22, 2024

Abstract

This study introduces an innovative methodology for mortality forecasting, which integrates signature-based methods within the functional data framework of the Hyndman-Ullah (HU) model. This new approach, termed the Hyndman-Ullah with truncated signatures (HUTs) model, aims to enhance the accuracy and robustness of mortality predictions. By utilizing signature regression, the HUTs model aims to capture complex, nonlinear dependencies in mortality data which enhances forecasting accuracy across various demographic conditions. The model is applied to mortality data from 12 countries, comparing its forecasting performance against classical models like the Lee-Carter model and variants of the HU models across multiple forecast horizons. Our findings indicate that overall the HUTs model not only provides more precise point forecasts but also shows robustness against data irregularities, such as those observed in countries with historical outliers. The integration of signature-based methods enables the HUTs model to capture complex patterns in mortality data, making it a powerful tool for actuaries and demographers. Prediction intervals are also constructed using bootstrapping methods.

Keywords: Hyndman-Ullah model, Lee-Carter model, principal component analysis, functional data analysis

1 Introduction

Mortality modeling and forecasting are quintessential to the disciplines of actuarial science, demography, and public health, serving as critical tools for socio-economic planning and risk management. The primary objective

of mortality forecasts is to provide reliable estimates of future mortality rates and life expectancies, which shape various policy and financial strategies. Understanding and anticipating mortality trends is fundamental for government agencies to adequately plan and allocate resources in healthcare, social security, and public welfare sectors. As populations age and demographic shifts occur, precise mortality forecasts are indispensable for sustainable public policy and healthcare system planning to guide governments in making informed decisions about retirement ages, healthcare funding, and pensions, ensuring that social security systems remain robust in the face of demographic changes.

In the insurance and pension industries, mortality modeling takes part in the pricing of life insurance and annuities, as well as the management of pension funds. Actuaries rely on these models to calculate premiums, reserves, and pension contributions that align with predicted mortality rates, thus safeguarding the financial health of these institutions against longevity risks (Deprez et al., 2017). Moreover, accurate mortality projections are critical in the context of global challenges such as the increasing life expectancy, coupled with declining fertility rates in many parts of the world, poses additional challenges with the shifting age structure of populations. These demographic trends amplify the importance of mortality forecasting, as they have profound implications for the economic sustainability of pension systems and public health policies (Bjerre, 2022). Thus, the practice of mortality modeling and forecasting not only supports financial and actuarial operations but also facilitates broader strategic planning and policy-making that accommodate the evolving demographic landscapes, ultimately ensuring the economic and social stability of societies.

1.1 Mortality modelling and forecasting

Mortality models are broadly categorized into three approaches: expectation, explanation, and extrapolation (Booth and Tickle, 2008). Each serves distinct purposes in understanding and predicting mortality rates. The expectation approach relies on expert opinions to forecast mortality, emphasizing informed conjectures based on past experiences. Meanwhile, explanation models link mortality rates to various risk factors such as lifestyle or socioeconomic status, using regression techniques to uncover the underlying causes of mortality patterns. The primary focus, however, is on extrapolation, the most actively researched and commonly used approach, particularly by national statistical bureaus. This method projects future mortality rates based on the continuation of observed historical trends and age patterns. By leveraging time series analysis and other statistical techniques that emphasize trend continuity, extrapolative models provide robust forecasts grounded in the regularity of past data, making them indispensable for demographic analysis and policy planning.

The seminal work of Lee and Carter (1992) was undoubtedly one of the most influential extrapolative models to be introduced to forecasts mortality rates. The Lee-Carter (LC) model

$$\ln(m_{x,t}) = a_x + b_x k_t + e_{x,t},$$

is an age-period mortality model with a log-bilinear structure that models the logarithm of central death rates, $m_{x,t}$ with a location parameter a_x that accounts for the average logarithm of rates across the specified time period, a singular value decomposition derived bilinear term that captures the age pattern and mortality trends with a term that reflects the rate of mortality change of a particular age, b_x , and a mortality index that varies over time, k_t , and the error term $e_{x,t}$. Forecasts of the LC model are then produced by extrapolating the mortality index with time series methods where in most cases a random walk with drift would suffice. While the LC model was initially applauded for its simple structure and straightforward implementation, it did have its fair share of limitations which were subsequently addressed in various extensions of the LC model (Lee and Miller, 2001; Booth et al., 2002). Extensions were also not limited to adjustments to the original LC model as seen in the deployment of generalised linear models (Renshaw and Haberman, 2003) and Bayesian statistics (Czado et al., 2005). Readers are directed to Basellini et al. (2023) for a more recent review on LC methods since the introduction of the LC model.

The LC extension of interest in this paper involves the functional data paradigm (Ramsay and Silverman, 2005). The Hyndman-Ullah (HU) model (Hyndman and Ullah, 2007) is a generalisation of the LC model that uses concepts from functional data analysis to better model the mortality rates by exploring the variations within the data from a functional perspective. The use of nonparametric smoothing techniques on the age-specific mortality rates allowed for the removal of the LC model's homoskedasticity assumption and realise an underlying smooth curve that can be decomposed using functional principal component analysis with their orthonormal basis. Component wise it is similar to the LC model except it allows for multiple principal components to be included, accounting more variation into the model which Hyndman and Ullah (2007) noted is the reason for its superior performance for longer-term forecast. Comparisons also show that the HU model outperformed the LC, Lee-Miller, and Booth-Maindonald-Smith models. Recent extensions of the HU model have been for the modelling of subpopulations (Jiménez-Varón et al., 2024; Shang et al., 2022; Shang and Hyndman, 2017). In light of the substantial contributions made by the HU model, there is still a growing interest to explore new modifications to improve its efficacy and adaptability. This paper explores the integration of signatures into the HU model, to better capture the nonlinear patterns often present in mortality data of a single population. This approach seeks

to merge established statistical techniques with innovative mathematical insights, potentially enriching the analytical landscape of actuarial science.

1.2 Signatures from rough path theory

The signature is a sophisticated mathematical tool that is capable of summarising complex, high-dimensional data paths through their iterated integrals in an informative and compact package as a power series that contains the tensor coefficients. Originally introduced by Chen (1957) and further developed in the context of rough path theory by Lyons et al. (2007), they have found extensive applications across multiple fields, particularly where the analysis of dynamic systems is crucial. Their effectiveness has been demonstrated in various applications such as sepsis detection (Morrill et al., 2020), identifying Chinese handwriting (Xie et al., 2018), and in diagnosing psychological disorders (Wang et al., 2020). The increasing interest in signatures stems primarily from their ability to effectively condense information from complex sequences without losing critical details, making them exceptionally useful for detection work. This efficiency in capturing the essence of data paths while minimizing complexity is what drives their growing popularity, especially in areas dealing with large volumes of sequential data.

Signatures possess a unique mathematical property known as universal nonlinearity, which enables the application of regression techniques directly on these signature representations, known as signature regression. This method leverages the rich algebra provided by the signatures to model and predict dependent variables from a sequence of inputs. The practical implication of this is that it can construct predictive models that are capable of handling data with complex temporal dynamics and interactions. In other words, the universality of signatures means that any continuous function on the space of signatures can approximate continuous functions on the space of paths to an arbitrary degree of accuracy. This broad capability makes signature-based models exceptionally versatile and powerful, providing a robust framework for tackling problems where conventional regression models might struggle with the complexities of the data.

Signature regression is further highlighted through various applications across different fields. For instance, Levin et al. (2016) utilized the universal properties of signatures to characterize functional relationships within datasets, leading to the development of the expected signature model. This model leverages linear regression on signature features to summarize the conditional distribution of responses effectively. It has demonstrated superior forecasting abilities compared to autoregressive and Gaussian Process models, especially in scenarios involving large datasets, thereby highlighting its efficiency in data stream summarization and significant dimension reduction. Building on these foundations, Fermanian (2022) introduced the signature linear model within a functional regression framework. This model operates

by mapping functions to their signatures and employing ridge regression for prediction, showing enhanced capabilities in handling multidimensional data. By surpassing established methods like functional linear models and functional principal component regression, the signature linear model eliminates the need for certain assumptions typically required within functional settings, streamlining the modeling process.

Moreover, the adaptability and simplicity of modelling with signature regression have been elaborated by Cohen et al. (2023), who noted their effectiveness in simplifying time series modeling. This approach involves merely computing signatures from observed paths and applying regression, significantly reducing the complexity associated with time series analysis. The flexibility of signature methods also extends to handling missing data and irregular sampling, making them applicable for diverse forecasting and analysis tasks. Notably, when applied to nowcast the gross domestic product growth of the United States, signature regression methods have outperformed dynamic factor models, showcasing its potential in economic forecasting.

In the field of actuarial science, the use of signatures has started to make inroads, particularly in areas such as financial derivatives pricing (Lyons et al., 2020), risk management (Andrès et al., 2024), and optimal execution (Kalsi et al., 2020). However, the application of signatures in the life and mortality side of actuarial science remains less explored, indicating a gap for research and potential development. The introduction of signature regression into mortality forecasting presents a novel methodology that could improve the accuracy of predictions by leveraging the universality of signatures to effectively model complex, nonlinear relationships inherent in mortality data. It is therefore the aim of this article to introduce a functional mortality model by which is decomposed using truncated signatures in place of FPCA that also utilises the extrapolation method to produce forecasts. The model will from here on be referred to as the HU with truncated signatures (HUts) model and will be used to obtain point and interval forecasts of log mortality rates of several countries that are readily available from the Human Mortality Database (2024).

The remainder of this paper is structured as follows. Section 2 provides a description of the methodology, detailing the HU model and the integration of signature regression. Section 3 presents the empirical analysis, including data preparation and results of applying the proposed model to mortality data across various countries. In Section 4, we discuss the implications of these results, and section 5 concludes.

2 Methodology

2.1 The Hyndman-Ullah (HU) model

The HU model is a generalised extension of the Lee-Carter model, employing the functional data paradigm (Ramsay and Silverman, 2005) and nonparametric smoothing to improve the forecasting of mortality rates. This model is distinguished by its use of multiple principal components, capturing a broader variation within the data, and applying more advanced time series forecasting methods than the random walk with drift model typically used in the LC model (Hyndman and Ullah, 2007).

At its core, the HU model assumes that log mortality rates $y_t(x)$ observed at discrete ages x and years t have an underlying smooth function $f_t(x)$, observed with error:

$$y_t(x) = f_t(x) + \sigma_t(x)\epsilon_t,$$

where ϵ_t is the standard normal error term and $\sigma_t(x)$ denotes the observational standard deviation which is allowed to vary with age (Hyndman and Ullah, 2007). This lets the HU model handle data heterogeneity and ensures demographic consistency by applying monotonicity constraints when using penalized regression splines to smooth the mortality curves (Hyndman and Ullah, 2007).

Functional principal component analysis (FPCA) is used to decompose the smoothed mortality rates into principal components. By applying FPCA to the centered smooth mortality would yield:

$$f_t(x) = \mu(x) + \sum_{k=1}^K \beta_{t,k} \phi_k(x) + e_t(x).$$

Here, $\mu(x)$ represents the mean function, $\phi_k(x)$ are orthonormal basis functions, $\beta_{t,k}$ are time dependent coefficients, and $e_t(x)$ is the error function. Forecasts of mortality rates are done through the time dependent coefficients, $\beta_{t,k}$ which are fitted into univariate robust ARIMA models and extrapolated h -steps ahead.

A critical consideration in applying FPCA is its sensitivity to outliers. Extreme values can disproportionately influence the principal components derived from the data. This sensitivity may lead to biased or misleading results, especially when modeling phenomena such as mortality rates where spikes might occur due to extraordinary events like epidemics or wars. To address these issues, various adaptations of the HU model have been put forth. These include the robust HU (HUrob) model with robust FPCA (Hyndman and Ullah, 2007), which seeks to minimize the impact of outliers by using the L_1 -median as the location measure, paired with the reflection-based algorithm for principal components analysis (Hubert et al., 2002) for

a robust set of principal components; the weighted HU (wHU) model with weighted FPCA (Hyndman and Shang, 2009), which adjusts the influence of data points by placing more weight on recent data with the measure of location being a weighted average using geometrically decreasing weights. These modifications aim to enhance the stability and reliability of the model under conditions where data anomalies are present. Having the same goal in mind to make the model less sensitive to outliers, we extend the literature by exploring the use of signature regression on the signature of age specific mortality rates as an alternative to enhancing the robustness of mortality forecasts.

2.2 The signature of a path

2.2.1 The concept of signatures

In statistical analysis, particularly when dealing with time-series or sequential data, understanding the concept of a “path” is crucial. A path $X : [0, 1] \rightarrow \mathbb{R}^d$ is defined as a continuous mapping from an interval to a topological space, which is assumed to be piecewise differentiable and of bounded variation. Unlike time series or stochastic processes, which are explicitly governed by time, a path emphasizes its geometrical movements through space, making the term “path” more suitable. From a computational perspective, think of a path as input data with d dimensions, analogous to multi-dimensional time series data.

Signatures are mathematical tools used to encode the information contained in a path. Using Chen’s identity (Chen, 1957), the signature of a piecewise linear path is computed by taking the tensor product of exponentials of the linear segments of the path. Thus, the signature of a path, or simply signatures, is a collection of all iterated integrals between coordinates of a path. This collection is often described as an abstract summary of the input signal’s variability.

Definition 2.1 (Signature of a path (Fermanian, 2022)) *Let $X : [0, 1] \rightarrow \mathbb{R}^d$ be a path of bounded variation, and let $I = (i_1, \dots, i_k) \in \{1, \dots, d\}^k$, where $k \in \mathbb{N}^*$, be a multi-index of length k . The signature coefficient of X corresponding to the index I is defined by*

$$\begin{aligned} S^I(X) &= \int_{0 \leq u_1 < \dots < u_k \leq 1} \dots \int dX_{u_1}^{i_1} \dots dX_{u_k}^{i_k} \\ &= \int_0^1 \int_{u_1}^1 \int_{u_2}^1 \dots \int_{u_{k-1}}^1 dX_{u_k}^{i_k} \dots dX_{u_2}^{i_2} dX_{u_1}^{i_1}, \end{aligned}$$

where $S^I(X)$ is called the signature coefficient of order k . The signature of X is then the sequence containing all the signature coefficients:

$$S(X) = (1, S^{(1)}(X), \dots, S^{(d)}(X), S^{(1,1)}(X), \dots, S^{(i_1, \dots, i_k)}(X), \dots).$$

However, from a practical standpoint, it is not feasible to use all the signature coefficients in the infinite sequence of the signature of X due to computational limits, and also due to the factorial decay of the coefficients as the order increases (Bonnier et al., 2019). Therefore, it is often sufficient to consider the signature of a path up to a truncated order of m , denoted as:

$$S^m(X) = (1, S^{(1)}(X), \dots, S^{(d)}(X), S^{(1,1)}(X), \dots, S^{(i_1, \dots, i_m)}(X)),$$

which contains $\frac{d^{m+1}-1}{d-1}$ number of signature coefficients. Note that the number of signature coefficients grows exponentially with the truncation order.

A fundamental attribute of the signature is its ability to encode the geometric properties of a path. The first-order terms, $S^{(i)}(X)$, are straightforward, representing the total change along each dimension of the path or the increments observed in each variable. The second-order terms, $S^{(i_1, i_2)}(X)$, provide insights into the interaction between pairs of dimensions, similar to capturing the area enclosed by the path as it travels through these dimensions, and higher-order interactions are particularly valuable for understanding complex dependencies and dynamics within the data.

2.3 Embedding with signatures

Embedding paths before computing its signature is a standard practice used to maximise the potential of signatures by addressing inherent invariances such as translation and time reparametrization that can result in significant information loss. These embedding transformation ensure that all relevant information are preserved and encoded into the signature and in turn enrich the signature’s capability to reflect the complex dynamics within the path.

The basepoint augmentation (Kidger and Lyons, 2020) involves inserting a fixed initial point to the path data. By anchoring the sequence, basepoint augmentation allows the signature to overcome the translation invariance of the signature.

Time augmentation counteracts the signature’s invariance to time reparametrization, by introducing a monotone coordinate that serves as a virtual timestamp to each point in the path. This embeds precise temporal information into the path, making the signature sensitive to the sequence’s timing. Besides, this also guarantees the uniqueness of the signatures computed (Hamby and Lyons, 2010).

To further aid the sequential learning capabilities of the signature, the lead-lag transformation extends the path’s dimensionality by interleaving the original path with its lagged version, which enriches the data representation, allowing the signature to capture not only the path’s immediate direction but also its past states. Fermanian (2021) noted the lead-lag transformation improves a model’s predictive capabilities and is beneficial for tasks involving sequential data.

In the proceeding sections, we will use these embedding transformation to prepare our data paths before computing its signature so as to enhance the signatures' ability to capture and reflect the complex dynamics of the sequences.

2.4 Signature regression

One of the many practical applications of signatures are its usage as feature maps in a regression framework. This rich representation allows for the modelling of complex relationships within functional data. The ability of signatures to compactly encode information about paths makes them particularly powerful for handling high-dimensional and complex datasets, enabling the application of regression techniques in scenarios where conventional methods might be inadequate due to the complexity and dimensionality of the data. These are motivated and guaranteed by many results as pointed out by the shuffle identity, the signature approximation theorem (Levin et al., 2016) and the universal nonlinearity of paths (Bonnier et al., 2019).

Definition 2.2 (Universal nonlinearity (Bonnier et al., 2019)) *Let f be a real-valued continuous function on continuous piecewise smooth paths in \mathbb{R}^d and let κ be a compact set of such paths. Assume that $X_0 = 0, \forall X \in \kappa$, let $\epsilon > 0$, there exists a linear functional L such that,*

$$|f(X) - L(S(X))| < \epsilon.$$

Kiraly and Oberhauser (2019) then gathered that a linear combination of signature features are capable of approximating continuous functions arbitrarily well, meaning signatures are able to linearise functions of a path, further emphasizing the universality (Levin et al., 2016) of signatures. To further clarify, consider a classical regression setting with a path X that maps some space into \mathbb{R}^d and Y a response, we have

$$Y = f(X) + \epsilon,$$

where f is some functional that characterises the relationship between the response and the path. Assuming f is nonlinear, it is then generally challenging to determine the function f accurately due to the increased complexity in parameter estimation, model interpretation, and computational resources required for non-linear regression or possibly neural networks, compared to linear regression. However, if the signature of path X is considered as the predictors instead, we can redefine the relationship with a linear functional g such that

$$Y = g(S(X)) + \epsilon.$$

Although in theory linear regression is sufficient for estimating g , in practice, regularization techniques are used to handle the multicollinearity of signature features (Levin et al., 2016) as linear regression models can become unstable when variables are not independent. This instability often results in large variances in the estimated coefficients, making the model unreliable.

2.5 The Hyndman-Ullah model with truncated signatures

We are now prepared to integrate signatures into the Hyndman-Ullah (HU) model, which we will refer to as the HU with truncated signatures (HUTs) model. The integration of signatures with functional data models has been documented by Fermanian (2022) and Frévent (2023). However, these studies primarily applied signature regression in a functional regression framework with scalar responses and functional covariates, where signatures of the functional covariates were used directly. In contrast, the HU model operates more like a functional regression model with functional responses, making the direct application of signature regression more complex. We plan to consider using the signature of cross-sectional data from these functional covariates to apply signature regression at each point throughout the functional domain and then reconstruct a functional response. The HUTs model is presented as follows:

$$y_t(x) = f_t(x) + \sigma_t(x)\epsilon_t,$$

$$f_t(x) = \mu(x) + \sum_{k=1}^K \beta_{t,k} Z_k(x) + e_t(x),$$

where $Z_k(x)$ is the k^{th} principal component of the signature of the transformed path of age specific rates, and its respective scores $\beta_{t,k}$.

The smoothing approach of the mortality rates are remained as the original HU model, which is with the constrained weighted penalized regression splines to obtain $\hat{f}_t(x)$. This ensures the model retains the capacity to account for handling heteroskedasticity in mortality data as variability is different across different ages or time periods. Although more advanced smoothing techniques such as bivariate smoothing (Dokumentov et al., 2018) have been put forth, they also introduce additional complexity and computational demands.

Additionally, the estimation of the mean function is also kept the same as in the HU model, by averaging all the smoothed curves:

$$\hat{\mu}(x) = \frac{1}{n} \sum_{t=1}^n \hat{f}_t(x).$$

This method provides a straightforward and effective way to capture the central tendency of the functional responses. Now we will decompose the

centered curves, $f_t^*(x) = \hat{f}_t(x) - \hat{\mu}(x)$ with signature regression over a fine grid of q equally spaced values $x_1^*, \dots, x_q^* \in [x_1, x_p]$.

Consider the time series of the smoothed mortality rates for age x_i , $\{\hat{f}_t(x_i)\}_{t=1}^n$. Combining the basepoint augmentation, time augmentation, and the lead-lag transformation, the augmented path can be transformed as follows:

$$\tilde{X}_i = \left((t_0, 0, 0), (t_1, \hat{f}_1(x_i), \hat{f}_1(x_i)), (t_2, \hat{f}_2(x_i), \hat{f}_1(x_i)), (t_3, \hat{f}_2(x_i), \hat{f}_2(x_i)), \right. \\ \left. (t_4, \hat{f}_3(x_i), \hat{f}_2(x_i)), \dots, (t_n, \hat{f}_n(x_i), \hat{f}_n(x_i)) \right),$$

where t is an ordered sequence within the interval $[0, 1]$ where $t_0 = 0 < t_1 < t_2 < \dots < t_n = 1$, marking the times of observations. This structured augmentation ensures that each data point x_i is not only represented by its current value but also linked to its immediate past, enhancing the path's dimensionality and capturing both the direction and history within the data, thereby enriching the data representation for signature computation. The transformed time series \tilde{X}_i is then used to compute the truncated signature $S^m(\tilde{X}_i)$.

To estimate $\beta_{t,k}$, we then set up our signature regression framework:

$$f_t^*(x) = g_t(S^m(\tilde{X}_i)) + \hat{\epsilon}_t(x_i)$$

for some linear function g_t , which we will use principal component regression to solve. Applying PCA helps by reducing the dimensionality of the signature coefficient feature space to a smaller set of k uncorrelated principal components denoted as $Z_k(x_i)$. This reduction not only simplifies the model but also enhances its stability and efficiency by focusing on the most informative aspects of the dependency within the signatures. Additionally, using PCA aids in orthogonalizing the terms, which simplifies the calculation of forecast variance later and resembles the approaches used in both the original HU and LC models.

For computational simplicity, we define the matrices

$$S = \begin{bmatrix} S^m(\tilde{X}_1) \\ \vdots \\ S^m(\tilde{X}_q) \end{bmatrix}_{q \times s_d(m)}, \quad Y_t = \begin{bmatrix} f_t^*(x_1) \\ \vdots \\ f_t^*(x_q) \end{bmatrix}_{q \times 1}.$$

We then apply PCA to obtain the orthogonal principal component scores by singular value decomposition, $S = U\Sigma V^T$ where the first K principal component scores are the first K columns of $Z = U\Sigma$. Then, to obtain $\hat{\beta}_t$ is equivalent to solving

$$\hat{\beta}_t = (Z_K^T Z_K)^{-1} Z_K^T Y_t,$$

where Z_K is a $q \times K$ matrix where the i^{th} row contains the normalised principal component of the truncated signature of order m of age x_i ,

By combining everything together we have

$$\hat{f}_t(x) = \hat{\mu}(x) + \sum_{k=1}^K \hat{\beta}_{t,k} \hat{Z}_k(x) + \hat{e}_t(x),$$

where $\hat{Z}_k(x)$ is obtained via interpolation.

2.6 Forecasting with the HUts model

2.6.1 Point forecast

Similar to that of the HU model, the time dependent coefficients are extrapolated by fitting them into univariate time series $\{\hat{\beta}_{t,k}\}_{t=1}^n$. We preserve the choice of using univariate robust ARIMA models (Chen and Liu, 1993) as in the HU model to forecast each coefficient h -steps ahead, $\hat{\beta}_{n+h|n,k}$, for each $k = 1, \dots, K$. Subsequently, the forecasted log mortality rates can be calculated with:

$$\hat{y}_{n+h|n}(x) = \hat{\mu}(x) + \sum_{k=1}^K \hat{\beta}_{n+h|n,k} \hat{Z}_k(x).$$

Since each term is constructed to be orthogonal to one another, the forecast variance can also be approximated, assuming all sources of error are normally distributed, by summing of the component variances similar to that of the forecast variance of the HU model (Hyndman and Ullah, 2007):

$$\text{Var}(y_{n+h|n}(x)) \approx \hat{\sigma}_\mu^2(x) + \sum_{k=1}^K \hat{Z}_k^2(x) u_{n+h|n,k} + v(x) + \sigma_{n+h|n}^2(x), \quad (2.1)$$

where $\hat{\sigma}_\mu^2(x)$ is the variance obtained from estimating the mean function, $u_{n+h|n,k}$ is the variance from the time series used to forecast $\hat{\beta}_{n+h|n,k}$, $v(x)$ are model fit errors which is estimated by averaging $\hat{e}_t(x)$, and finally $\sigma_{n+h|n}^2(x)$, the observational variance.

2.6.2 Interval forecast

Obtaining prediction intervals is essential because they provide a measurable indication of the uncertainty in forecasts. Prediction intervals quantify the range within which future observations are likely to occur, at a specified confidence level. This allows evaluation of the reliability of predictions when model uncertainty is significant, as different models may offer varying forecasts performance. Chatfield (1993) emphasized the importance of prediction intervals for evaluating future uncertainty, preparing for various

scenarios, comparing different forecasting methods, and exploring outcomes under different assumptions. By providing a range of possible outcomes, interval forecasts allow policymakers and researchers to prepare for a variety of future scenarios, thus enhancing the reliability of their strategies against unexpected changes. For example, understanding the variability in future mortality rates can profoundly impact the structuring of insurance (Hyndman and Shang, 2009). Interval forecasts help insurers assess the risk associated with different demographic scenarios, which is then translated into premiums to reflect the uncertainty of their projections. This further frames the concept of interval forecasts as a fundamental component in the field of demography.

Constructing prediction intervals is straightforward under the assumption that all sources of error are uncorrelated and normally distributed. Using the standard normal distribution, these intervals can be easily derived by applying quantile values to scale the forecast standard deviation obtained in Equation (2.1) which is straightforward to implement. However, its accuracy heavily depends on the validity of the normality assumption. If the normality assumption is violated, the prediction intervals may not be accurate, suggesting that a nonparametric bootstrap procedure would be more practical.

2.6.3 Bootstrap prediction interval

As the normality assumption is not satisfied (see A.1 in the Appendix) for the HUtS model, we employ Hyndman and Shang (2009)'s method to construct the bootstrap prediction intervals.

The procedure begins by utilizing univariate time series models to generate multi-step-ahead forecasts for the scores of principal components, $\{\beta_{1,k}\}_{t=1}^n$. Subsequently, for $t = h + 1, \dots, n$, we calculate the forecast errors for h -step-ahead forecasts as:

$$\hat{\xi}_{t,h,k} = \hat{\beta}_{t,k} - \hat{\beta}_{t|t-h,k}.$$

To create a bootstrap sample of $\beta_{n+h,k}$, we randomly resample these forecast errors with replacement, designated as $\hat{\xi}_{*,h,k}^{(l)}$, and add them to the h -step-ahead forecast, $\hat{\beta}_{n+h|n,k}$, yielding:

$$\hat{\beta}_{n+h|n,k}^{(l)} = \hat{\beta}_{n+h|n,k} + \hat{\xi}_{*,h,k}^{(l)},$$

for $l = 1, \dots, L$.

The model's residual, $\{e_t(x)\}$ is bootstrapped from the residuals $\{\hat{e}_1(x), \dots, \hat{e}_n(x)\}$ by sampling with replacement. Similarly, smoothing errors $\hat{\epsilon}_{n+h,i}^{(l)}$ can be bootstrapped by resampling with replacement from $\{\hat{\epsilon}_{1,i}, \dots, \hat{\epsilon}_{n,i}\}$.

When constructing the L variants for $\hat{y}_{n+h|n}^{(l)}(x)$, all possible components of variability are combined, assuming they are uncorrelated to each other

by using:

$$\hat{y}_{n+h|n}^{(l)}(x) = \hat{\mu}(x) + \sum_{k=1}^K \hat{\beta}_{n+h|n,k}^{(l)} Z(x) + \hat{\epsilon}_n^{(l)} + \hat{\sigma}_{n+h}(x) \hat{\epsilon}_{n+h,i}^{(l)}.$$

The prediction intervals are then derived from these bootstrap variants using their percentiles.

Bias corrected bootstrap prediction intervals

The bootstrap method, while powerful, can introduce systematic biases due to its reliance on resampling operations. These biases may result from the resampling process not perfectly replicating the underlying population characteristics. Therefore, Efron and Tibshirani (1993) introduced the bias correction, to address these inaccuracies by adjusting the bootstrap intervals. This adjustment ensures that the intervals are correctly centered around the point forecasts, potentially producing more reliable intervals, particularly when the data does not conform to normal distribution assumptions (Efron and Tibshirani, 1993). This correction is applied to the bootstrap prediction intervals by a correction factor, \hat{z}_0 , using the point forecasts.

$$\hat{z}_0 = \Phi^{-1} \left(\frac{\sum_{l=1}^L \mathbf{1}(\hat{y}_{n+h|n}^{(l)}(x) < \hat{y}_{n+h|n}(x))}{L} \right),$$

where $\mathbf{1}(\cdot)$ is the indicator function, and Φ is the distribution function of the standard normal distribution for $l = 1, \dots, L$. This factor calculates the proportion of bootstrap variants that are less than the point forecast and then subsequently transformed using the inverse standard normal distribution function. Then, to determine the adjusted percentiles, we use:

$$\alpha_1 = \Phi(\hat{z}_0 + z_{\alpha/2}), \quad \alpha_2 = \Phi(\hat{z}_0 + z_{1-\alpha/2}).$$

These calculations yield the adjusted percentiles α_1 and α_2 , which are used to construct the bias corrected prediction interval. This interval can effectively adjust for bias observed in the bootstrap sample, improving the accuracy of the predictive model's interval estimates, and more accurately reflect the true variability and bias of the forecast.

3 Empirical analysis

3.1 Data description

This study utilised datasets from 12 different countries, all sourced from the Human Mortality Database (2024). Of the 12 countries considered, data

Table 1: Mortality data by country

Country	Commencing Year	Age Range
Australia	1921	0-100+
Belgium	1920	0-100+
Bulgaria	1947	0-100+
Denmark	1899	0-99+
Finland	1899	0-96+
France	1899	0-100+
Ireland	1950	0-100+
Italy	1899	0-100+
Japan	1947	0-100+
Netherlands	1899	0-99+
Norway	1899	0-100+
United States	1933	0-100+

spanning all available years up to 2015 were extracted, with age groups ranging from zero to a carefully determined maximum age to avoid zero or missing values in elderly data. For ages beyond this established maximum, they were combined into an upper age group. In addressing intermediate missing values within the data for Denmark, Finland and Norway, a uniform approach was applied. A constant, represented by the smallest death rate value in the dataset, was added to each death rate prior to taking its logarithm. This adjustment facilitated a consistent treatment of missing values across the dataset. The selected countries are tabulated in Table 1, along with the commencing years and age groups.

3.2 Point forecast

The log mortality rates of 12 countries were forecasted with the HUts model using a truncation order $m = 2$ (see A.2 in the Appendix). It is therefore intuitive to compare the forecast accuracy of the proposed method with the HU model, HUrob model, wHU model, and the LC model, which are commonly used on mortality rates of a single population. For the HUts model and the HU model variants, the number of principal components, K is set to 6 which should be more than the required number of components considering the HU model is insensitive to the choice of K , presuming that K is large enough (Hyndman and Booth, 2008). The models were fitted using an expanding window approach, incorporating data from the respective commencing years of each country as outlined in Table 1. The initial forecasting period covers the most recent two decades which ends at 2015. We fit this

data using both models and produce forecasts up to ten-years ahead. The accuracy of these forecasts are then evaluated. Subsequently, the fitting period is then extended by one year and recalculate the forecasts for the same horizons. This procedure of expanding the training window continues until it includes data up to the year 2014.

In order to gauge the accuracy of the point forecast of the proposed signature mortality model, the mean squared error (MSE) and mean absolute error (MAE) are calculated and compared with the forecasts from the HU model. MSE quantifies the average squared difference between predicted and observed values, providing a measure of the overall accuracy and precision of predictions. On the other hand, MAE expresses the average difference between predicted and observed values. Both error measures can provide valuable insights into the model's overall accuracy, with lower values indicating better forecasting performance. The MSE and MAE are computed using:

$$\begin{aligned} MSE(h) &= \frac{1}{pq} \sum_{t=1}^q \sum_{i=1}^p (y_t(x_i) - \hat{y}_{t|t-h}(x_i)), \\ MAE(h) &= \frac{1}{pq} \sum_{t=1}^q \sum_{i=1}^p |y_t(x_i) - \hat{y}_{t|t-h}(x_i)|, \end{aligned} \tag{3.1}$$

where h is the forecasting horizon, p is the number of ages, q is the number of years considered in the forecasting period, $y_t(x_i)$ is the observed log mortality, and $\hat{y}_{t|t-h}(x_i)$ is the predicted value.

Table 2 and Table 3 present the MSE and MAE for one-step-ahead forecasts for each country using the different models. The results indicate that while the wHU model often achieves the lowest MSE and MAE values for one-step-ahead forecasts, the HUtS model still performs competitively, frequently achieving values close to the best-performing models. In comparison, the LC model shows significantly higher error rates, followed by the HU model and the HUrob model.

Table 2: MSE of one-step-ahead point forecasts of log mortality rates by method and country

	HUts	HU	HUrob	wHU	LC
Australia	0.00982	0.01027	0.01696	0.00952	0.10485
Belgium	0.02183	0.02144	0.02419	0.02047	0.18292
Bulgaria	0.01942	0.02131	0.02158	0.01968	1.08953
Denmark	0.03636	0.03810	0.04098	0.03590	0.11113
Finland	0.03856	0.04271	0.04435	0.03705	0.62800
France	0.00398	0.00642	0.00710	0.00399	0.15394
Ireland	0.05062	0.05174	0.05735	0.05161	0.10004
Italy	0.00711	0.00920	0.01600	0.00680	0.25442
Japan	0.00674	0.00747	0.00938	0.00687	0.11939
Netherlands	0.01242	0.01344	0.01569	0.01143	0.08333
Norway	0.04397	0.04303	0.04800	0.04264	0.56083
United States	0.00133	0.00207	0.00535	0.00129	0.01261
Mean	0.02101	0.02227	0.02558	0.02061	0.28341

Table 3: MAE of one-step-ahead point forecasts of log mortality rates by method and country

	HUts	HU	HUrob	wHU	LC
Australia	0.06111	0.06614	0.09498	0.06036	0.23231
Belgium	0.08404	0.09092	0.10116	0.08193	0.30475
Bulgaria	0.09106	0.10052	0.09727	0.09138	0.57395
Denmark	0.11169	0.12029	0.12909	0.11127	0.22268
Finland	0.11279	0.12608	0.13552	0.10976	0.55369
France	0.04246	0.06100	0.06336	0.04256	0.28411
Ireland	0.12512	0.13419	0.14838	0.12719	0.22055
Italy	0.05330	0.06842	0.08936	0.05210	0.34423
Japan	0.05061	0.05701	0.06955	0.04975	0.27212
Netherlands	0.06802	0.07839	0.08692	0.06657	0.20192
Norway	0.11718	0.11890	0.13299	0.11479	0.52488
United States	0.02648	0.03459	0.05380	0.02628	0.08755
Mean	0.07866	0.08804	0.10020	0.07783	0.31856

For five-step-ahead forecasts, the HUts model demonstrates more competitive performance. Table 4 and Table 5 show that overall the HUts model achieves lower error metrics compared to other models, particularly in contrast to the LC model. This suggests an improvement in the HUts model's forecasting ability as the horizon increases.

Table 4: MSE of five-step-ahead point forecasts of log mortality rates by method and country

	HUts	HU	HUrob	wHU	LC
Australia	0.01835	0.02245	0.02890	0.01642	0.11772
Belgium	0.02627	0.02863	0.03211	0.02620	0.20303
Bulgaria	0.04595	0.05212	0.04574	0.05478	0.59795
Denmark	0.04891	0.05484	0.05764	0.05007	0.08655
Finland	0.04698	0.05988	0.05328	0.04538	0.69713
France	0.00882	0.02290	0.01489	0.00978	0.15429
Ireland	0.07035	0.07198	0.07707	0.07785	0.11353
Italy	0.01625	0.03153	0.02982	0.01546	0.25481
Japan	0.01045	0.01288	0.01361	0.01020	0.21069
Netherlands	0.01785	0.02171	0.02374	0.01859	0.07366
Norway	0.05056	0.05309	0.05856	0.05053	0.58555
United States	0.00746	0.00900	0.01252	0.00896	0.01848
Mean	0.03068	0.03675	0.03732	0.03202	0.25945

Table 5: MAE of five-step-ahead point forecasts of log mortality rates by method and country

	HUts	HU	HUrob	wHU	LC
Australia	0.09131	0.11006	0.12925	0.08682	0.25691
Belgium	0.10163	0.11696	0.12482	0.10307	0.32362
Bulgaria	0.15511	0.17190	0.15103	0.15636	0.44353
Denmark	0.14989	0.16413	0.17112	0.15113	0.20720
Finland	0.14040	0.17654	0.15844	0.13800	0.59051
France	0.07102	0.12234	0.09527	0.07427	0.29203
Ireland	0.16031	0.18212	0.18869	0.17752	0.24991
Italy	0.09528	0.14200	0.13301	0.08831	0.35423
Japan	0.07659	0.08745	0.08784	0.07277	0.36327
Netherlands	0.09511	0.11317	0.11668	0.09702	0.19762
Norway	0.13801	0.15506	0.16166	0.13688	0.54332
United States	0.06428	0.07333	0.08508	0.06843	0.10677
Mean	0.11158	0.13459	0.13357	0.11255	0.32741

The results for ten-step-ahead forecasts, shown in Table 6 and Table 7, further confirm the strong performance of the HUts model. It consistently

Table 6: MSE of ten-step-ahead point forecasts of log mortality rates by method and country

	HUts	HU	HUrob	wHU	LC
Australia	0.0418	0.0511	0.0509	0.0351	0.1432
Belgium	0.0364	0.0380	0.0450	0.0404	0.2171
Bulgaria	0.0976	0.0931	0.0811	0.1280	0.1733
Denmark	0.0764	0.0825	0.0927	0.0825	0.0767
Finland	0.0653	0.0894	0.0773	0.0617	0.7650
France	0.0201	0.0526	0.0278	0.0242	0.1474
Ireland	0.1111	0.1297	0.1177	0.1413	0.1320
Italy	0.0403	0.0603	0.0594	0.0433	0.2481
Japan	0.0348	0.0399	0.0289	0.0362	0.3664
Netherlands	0.0326	0.0391	0.0406	0.0377	0.0513
Norway	0.0695	0.0775	0.0802	0.0718	0.5473
United States	0.0226	0.0196	0.0342	0.0305	0.0247
Mean	0.0540	0.0644	0.0613	0.0611	0.2410

Table 7: MAE of ten-step-ahead point forecasts of log mortality rates by method and country

	HUts	HU	HUrob	wHU	LC
Australia	0.1483	0.1705	0.1749	0.1383	0.2937
Belgium	0.1323	0.1421	0.1558	0.1434	0.3430
Bulgaria	0.2490	0.2389	0.2093	0.2341	0.2801
Denmark	0.2097	0.2182	0.2352	0.2151	0.2077
Finland	0.1804	0.2334	0.2105	0.1754	0.6260
France	0.1150	0.1905	0.1360	0.1204	0.2950
Ireland	0.2164	0.2663	0.2510	0.2641	0.2905
Italy	0.1623	0.2056	0.2019	0.1550	0.3655
Japan	0.1410	0.1536	0.1289	0.1435	0.4753
Netherlands	0.1448	0.1601	0.1637	0.1564	0.1820
Norway	0.1809	0.2089	0.2087	0.1837	0.5392
United States	0.1121	0.1122	0.1380	0.1250	0.1259
Mean	0.1660	0.1917	0.1845	0.1712	0.3353

achieves lower or comparable error metrics, reinforcing its effectiveness in long-term mortality rate forecasting. In most countries, the HUts model has lower MSE and MAE values, with exceptions in a few cases such as the United States, where the HU model occasionally performs better. This consistent performance across a majority of countries highlights the robustness

of the HUs model in capturing long-term trends in mortality rates.

Across different forecasting horizons, the best model is generally a choice between the HUs and wHU models, as these models tend to have the lowest error metrics. The wHU model performs better at shorter forecast horizons, as seen in the one-step-ahead results. However, as the forecasting horizon increases, the HUs model demonstrates improved performance and eventually surpasses the wHU model. This shift indicates that the HUs model’s accuracy and reliability become more pronounced with longer-term forecasts.

Notably, in the cases of France and Ireland, the HUs model performs consistently well across all forecasting horizons, maintaining lower MSE and MAE values compared to other models. Conversely, for Australia, the HUs model does not appear to be the most favorable at any point across the forecast horizons, with other models, such as wHU, often yielding better results. The following section will take a closer look at the mortality rate forecasts for France and Australia, exploring the nuances and potential reasons behind the differing performances of the HUs model against the HU variants. The LC model is excluded to ensure the plot scales remain appropriate and comparisons between the other models are more visible.

3.2.1 A closer look at the French and Australian mortality data

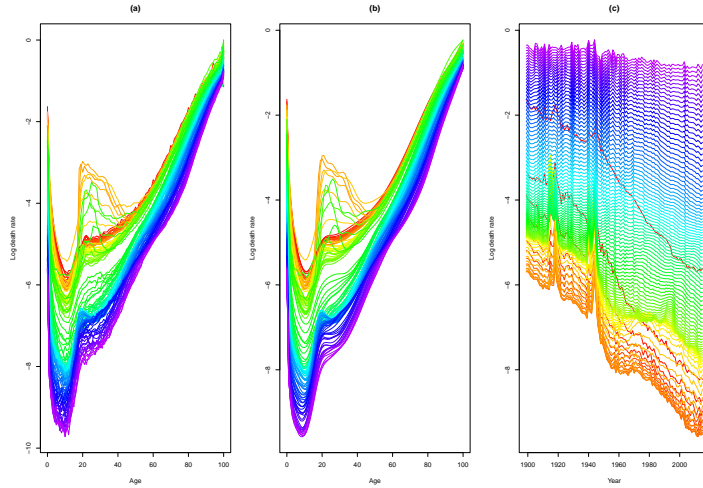


Figure 1: France (1899 to 2015); (a) Observed log mortality rates; (b) Smoothed log mortality rates; (c) Times series for ages

To assess the robustness of the HUs model, we examine the mortality rates of France and Australia more closely. Figures 1 (a) and 2 (a) include the observed log mortality rates, and Figures 1 (b) and 2 (b) show the smoothed log mortality rates with red representing the earlier years. Figures 1 (c) and 2 (c) the smoothed log mortality rates viewed as a time series with

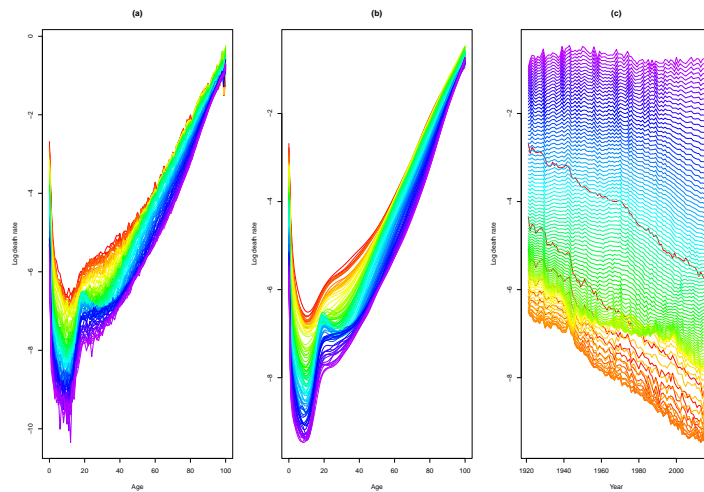


Figure 2: Australia (1921 to 2015); (a) Observed log mortality rates; (b) Smoothed log mortality rates; (c) Times series for ages

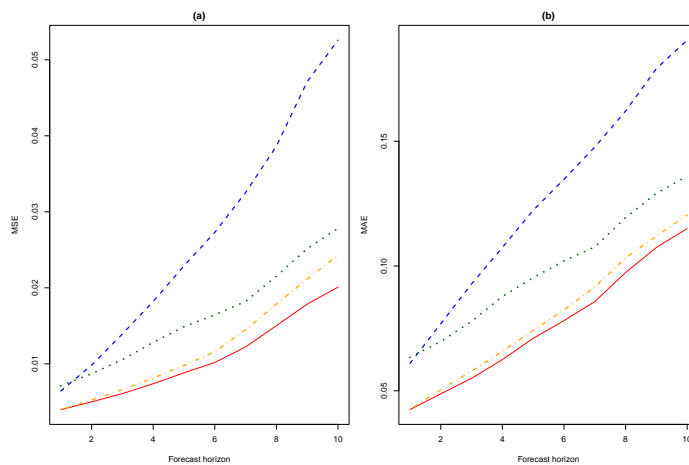


Figure 3: (a) MSE and (b) MAE plots for French mortality of the HUts (red solid line), HU (blue dashed line), HUrob (green dotted line), and the wHU (orange dash-dotted line) models

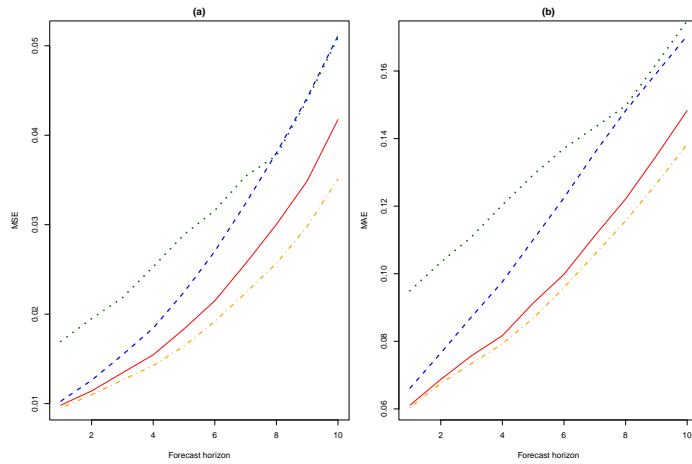


Figure 4: (a) MSE and (b) MAE plots for Australian mortality of the HUts (red solid line), HU (blue dashed line), HUrob (green dotted line), and the wHU (orange dash-dotted line) models

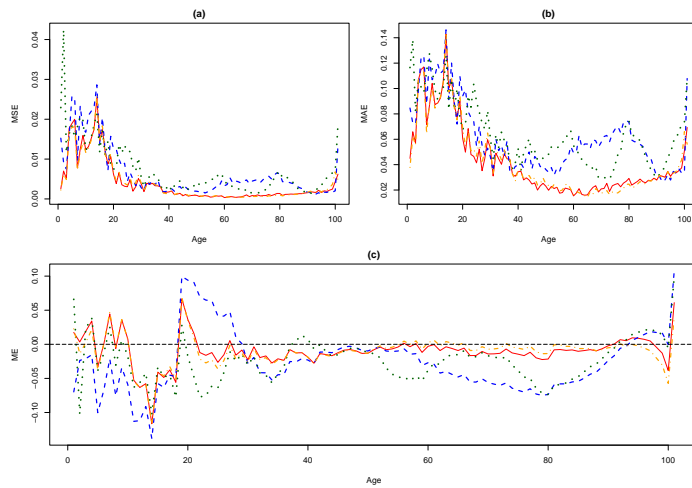


Figure 5: One-step-ahead (a) MSE and (b) MAE (c) ME plots averaged over years in forecasting period of French mortality of the HUts (red solid line), HU (blue dashed line), HUrob (green dotted line), and the wHU (orange dash-dotted line) models. A horizontal line at 0 is included in the ME plot to facilitate the assessment of forecast bias

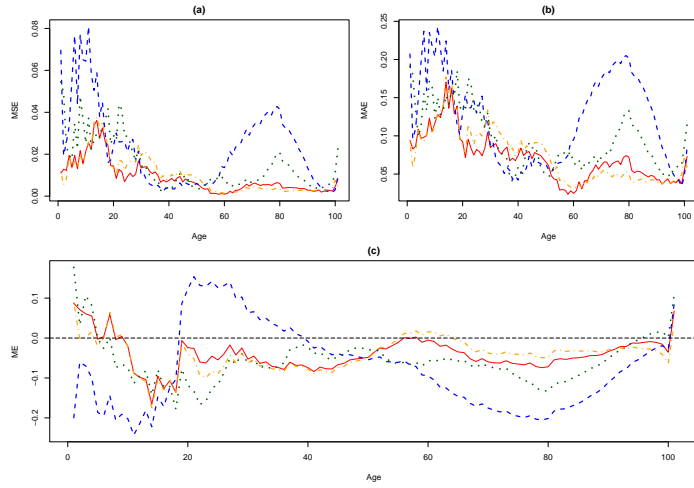


Figure 6: Five-step-ahead (a) MSE and (b) MAE (c) ME plots averaged over years in forecasting period of French mortality of the HUts (red solid line), HU (blue dashed line), HUrob (green dotted line), and the wHU (orange dash-dotted line) models. A horizontal line at 0 is included in the ME plot to facilitate the assessment of forecast bias

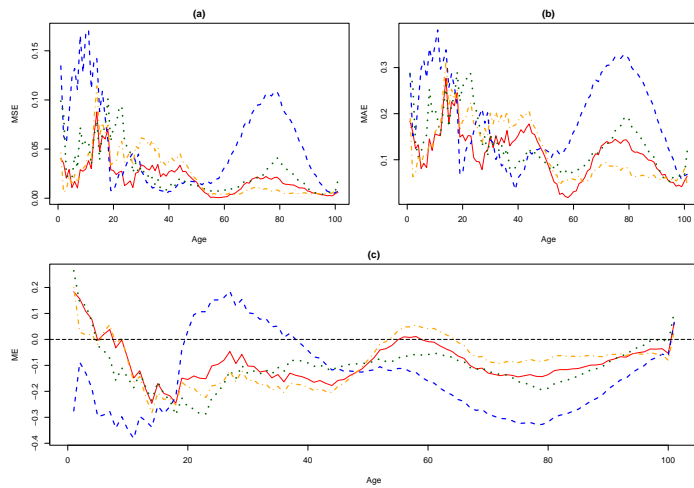


Figure 7: Ten-step-ahead (a) MSE and (b) MAE (c) ME plots averaged over years in forecasting period of French mortality of the HUts (red solid line), HU (blue dashed line), HUrob (green dotted line), and the wHU (orange dash-dotted line) models. A horizontal line at 0 is included in the ME plot to facilitate the assessment of forecast bias

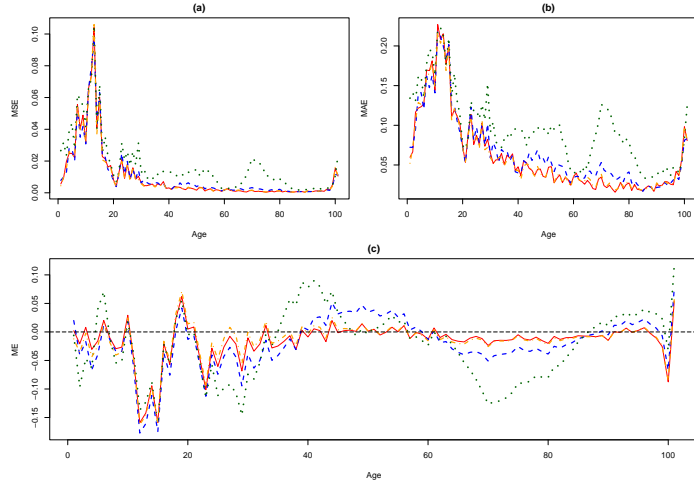


Figure 8: One-step-ahead (a) MSE and (b) MAE (c) ME plots averaged over years in forecasting period of Australian mortality of the HUts (red solid line), HU (blue dashed line), HUrob (green dotted line), and the wHU (orange dash-dotted line) models. A horizontal line at 0 is included in the ME plot to facilitate the assessment of forecast bias

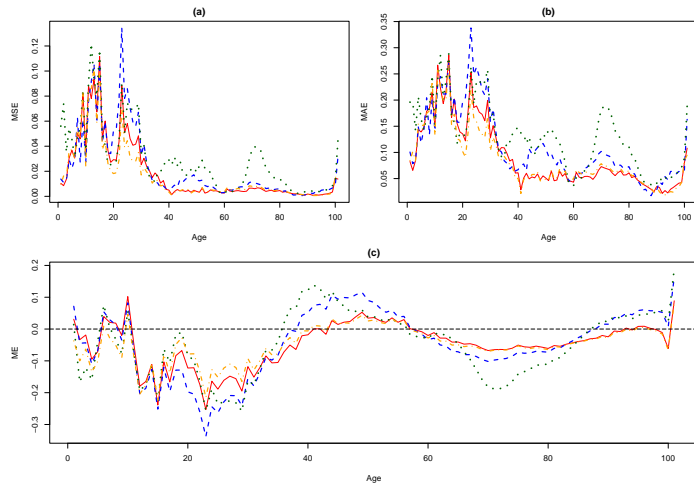


Figure 9: Five-step-ahead (a) MSE and (b) MAE (c) ME plots averaged over years in forecasting period of Australian mortality of the HUts (red solid line), HU (blue dashed line), HUrob (green dotted line), and the wHU (orange dash-dotted line) models. A horizontal line at 0 is included in the ME plot to facilitate the assessment of forecast bias

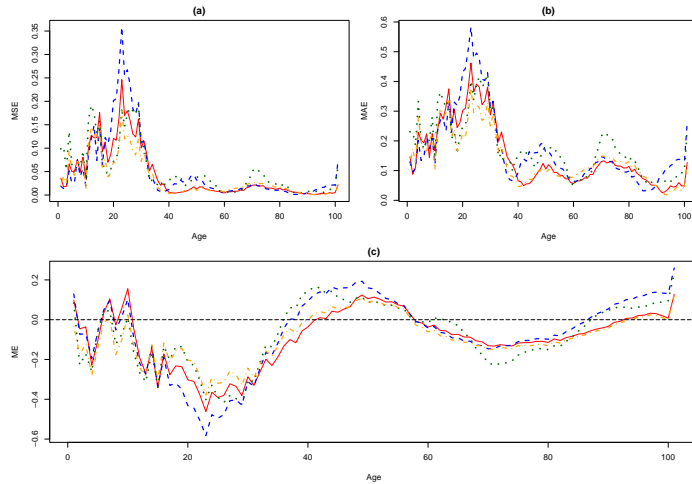


Figure 10: Ten-step-ahead (a) MSE and (b) MAE (c) ME plots averaged over years in forecasting period of Australian mortality of the HUts (red solid line), HU (blue dashed line), HUrob (green dotted line), and the wHU (orange dash-dotted line) models. A horizontal line at 0 is included in the ME plot to facilitate the assessment of forecast bias

red representing the earlier ages. France’s mortality data, notably influenced by periods of war and disease outbreaks, presents distinct outliers which are evident in the volatility observed in their mortality trends, as shown in Figure 1 which are most visible around the 1920s and 1940s. This provides an opportunity to test for the HUts model’s ability to handle anomalies in data. In contrast, Australia’s mortality data, starting from 1921 appears to have a smoother trend, without any significant outliers as depicted in Figure 2.

The ability of the HUts model to effectively handle anomalies in French mortality is illustrated in Figure 3, where the model demonstrates a substantial reduction in MSE and MAE across various forecast horizons when compared to the HU model. This significant improvement shows the HUts model’s robustness against data irregularities, making it a reliable choice for forecasting in scenarios with potential outliers. Additionally, the HUts model showcases lower MSE and MAE than both the HUrob and wHU models, further affirming its superior performance in handling French mortality data. Conversely, Australia presents a more stable dataset with mortality rates following a consistent trend and lacking significant outliers. The MSE and MAE plots for Australia in Figure 4 show less pronounced differences compared to France. While the HUts model demonstrates superior performance over the HU and HUrob models, affirming its effectiveness even in more uniform datasets, the wHU model performs better than the HUts

model. This suggests that the wHU model might be more suited for datasets with consistent trends and fewer irregularities. This comparative analysis highlights the importance of selecting appropriate models based on the characteristics of the dataset, with the HUts model excelling in more variable datasets and the wHU model in more stable ones. The MSE and MAE plots of the remaining 10 countries can be found at A.3 in the Appendix.

To gain deeper insights into the model performance, the MSE and MAE values are considered across the age spectrum. Instead of using Equation (3.1), the MSE and MAE values are averaged only over the years of the forecasting period. This approach will allow us to observe how the models perform at different age groups, providing a more granular understanding of the forecast accuracy. Additionally, we will also calculate the mean error (ME) to identify whether the models tend to overpredict or underpredict mortality rates at specific ages. The MSE, MAE and ME are computed with the following:

$$\begin{aligned}
 MSE(h, x_i) &= \frac{1}{q} \sum_{t=1}^q (y_t(x_i) - \hat{y}_{t|t-h}(x_i))^2, \\
 MAE(h, x_i) &= \frac{1}{q} \sum_{t=1}^q |y_t(x_i) - \hat{y}_{t|t-h}(x_i)|, \\
 ME(h, x_i) &= \frac{1}{q} \sum_{t=1}^q (y_t(x_i) - \hat{y}_{t|t-h}(x_i)).
 \end{aligned}$$

Upon a closer inspection of the evaluation metrics across different age groups of the French mortality data in Figures 5, 6, and 7, the HUts model generally surpasses every other model in terms of forecasting performance. For one-step-ahead forecasts (Figure 5), the HUts and wHU models show similar performance in terms of MSE and MAE, with both models outperforming the HU and HUrob models. The HUts model particularly excels in forecasting ages between 20 and 40, where it demonstrates substantially lower error values compared to the wHU model. The ME plot indicates that the HUts model's forecasts are mostly unbiased across ages, though there are some dips around age 15 and peaks around ages 20 and 100. The wHU model shows a similar trend, while the HU and HUrob models generally underpredict mortality. For five-step-ahead forecasts (Figure 6), the HUts model continues to perform well, maintaining lower MSE and MAE values across most age groups compared to the other models. The HUts model shows improved performance at middle ages (30-50), while the HU and HUrob models, although better at these ages, struggle during early and older ages, contributing to their higher overall error metrics. The ME plot for the HUts model remains close to zero, indicating minimal bias, whereas

the wHU model exhibits similar trends, and the HU and HUrob models continue to underpredict mortality. For ten-step-ahead forecasts (Figure 7), the HUts model’s performance remains robust, achieving lower MSE and MAE values across most age groups. However, it still faces competition from the wHU model, which performs better in certain age ranges. The ME plot for the HUts model shows a slight bias at extreme ages, but overall, it maintains a near-zero mean error across most ages, suggesting accurate and unbiased forecasts. The HU and HUrob models exhibit larger biases, contributing to their higher error metrics. Overall, these observations suggest that while the HUts model performs exceptionally well, particularly as the forecast horizon increases, the wHU model also shows strong performance, especially at shorter forecast horizons. The choice between these models often depends on the specific age group and forecasting horizon, with the HUts model becoming more favorable as the horizon increases.

Similarly, the evaluation metrics for the Australian mortality data in Figures 8, 9, and 10 highlight the competitive nature of the HUts model, particularly at shorter forecast horizons. For one-step-ahead forecasts (Figure 8), the HUts model performs comparably to the wHU model, with both showing nearly identical MSE and MAE values. This indicates that the HUts model is highly effective at short-term forecasting. The ME plot reveals minimal bias across ages for the HUts model, similar to the wHU model, while the HU and HUrob models exhibit a tendency to underpredict mortality. At the five-step-ahead horizon (Figure 9), the HUts model continues to perform well but begins to show higher MSE and MAE values in the 20-40 age range compared to the wHU model. This underperformance in mid-age groups becomes more evident, reflecting some biases that start to emerge at this forecast horizon. The ME plot for the HUts model indicates underprediction biases in this age range, contributing to the increased error metrics. By the ten-step-ahead forecasts (Figure 10), the HUts model, although still competitive, shows further increased MSE and MAE values around ages 20-40. This trend underscores the model’s underprediction in this specific age group, significantly affecting the overall error metrics. Despite this, the HUts model maintains reasonable performance across other age groups, yet the wHU model generally achieves better results at these longer horizons. While the HUts model shows strong performance and remains competitive across various forecasting horizons, it tends to exhibit higher MSE and MAE values around ages 20-40, especially at longer horizons, due to underprediction. This suggests that the wHU model might be better suited for datasets with more consistent trends and fewer irregularities, particularly for longer-term forecasts.

The findings of French and Australian mortality data present a comparative analysis of the HUts model’s performance under differing demographic conditions and historical events influencing mortality data. While the HUts model is able to perform well in stable demographic conditions, its advan-

Table 8: Coverage probability of 95% bootstrapped prediction intervals (PI)

	Bootstrapped PI (%)	Bias-Corrected Bootstrapped PI (%)
Australia	83.86%	88.48%
Belgium	93.38%	95.27%
Bulgaria	88.86%	91.10%
Denmark	76.79%	83.15%
Finland	93.62%	93.12%
France	99.91%	99.85%
Ireland	83.53%	86.66%
Italy	98.94%	98.73%
Japan	96.50%	98.34%
Netherlands	97.11%	97.03%
Norway	84.57%	87.64%
United States	93.17%	95.25%

tages are particularly noticeable when confronting data with potential outliers, making it a robust tool for forecasting when compared with the HU variants and the LC model.

3.3 Interval forecast

To evaluate the interval forecasts, the empirical coverage probability is calculated using the following expression (Hyndman and Shang, 2009):

$$\frac{1}{qph} \sum_{t=1}^q \sum_{j=1}^h \sum_{i=1}^p \mathbf{1} \left(\hat{y}_{t+j|t}^{(\alpha/2)}(x_i) < y_{t+j}(x_i) < \hat{y}_{t+j|t}^{(1-\alpha/2)}(x_i) \right),$$

where $\mathbf{1}(\cdot)$ is the indicator function, and $\hat{y}_{t+j|t}^{(\alpha/2)}(x_i)$ is the $\alpha/2$ -quantile from the bootstrapped samples. It quantifies whether the intervals are adequately wide to encompass the actual observations at a specified nominal coverage of $1 - \alpha$. 95% and 80% prediction intervals are constructed for all the 12 countries and tabulated in Tables 8 and 9 respectively.

The 95% and 80% bootstrapped prediction intervals are tabulated in Table 8 and 9 respectively. Overall, the bias-correction approach significantly improves the empirical coverage probabilities, bringing them closer to the nominal coverage levels. This adjustment helps to ensure that the prediction intervals are more accurately capturing the true variability in

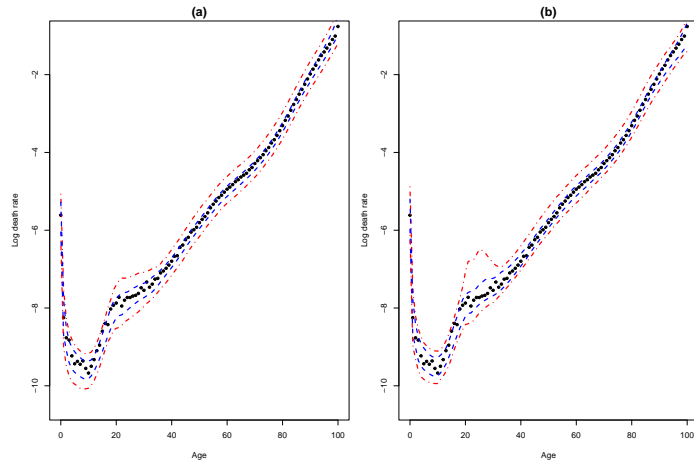


Figure 11: Bootstrapped 95% (red dot-dashed line) and 80% (blue dotted line) prediction intervals for one-step-ahead forecast for French mortality (1899-2014) (a) without bias correction (b) with bias correction

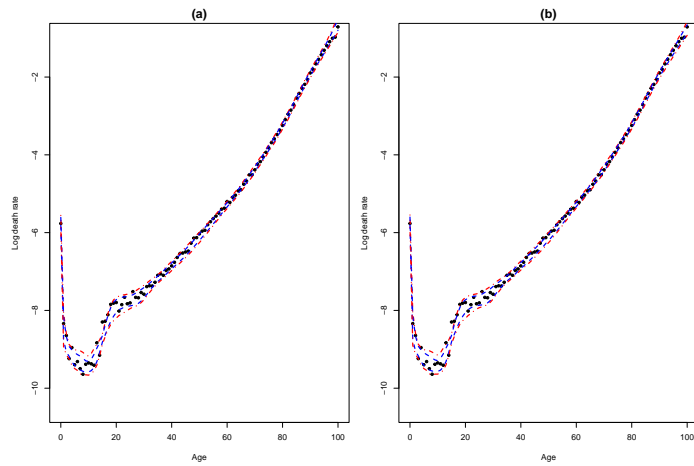


Figure 12: Bootstrapped 95% (red dot-dashed line) and 80% (blue dotted line) prediction intervals for one-step ahead forecast for Australian mortality (1974-2014) (a) without bias correction (b) with bias correction

Table 9: Coverage probability of 80% bootstrapped prediction intervals (PI)

	Bootstrapped PI (%)	Bias-Corrected Bootstrapped PI (%)
Australia	66.48%	74.25%
Belgium	78.72%	85.46%
Bulgaria	75.91%	78.40%
Denmark	55.97%	65.76%
Finland	82.25%	80.86%
France	97.29%	94.74%
Ireland	64.89%	76.93%
Italy	93.29%	91.24%
Japan	83.81%	95.71%
Netherlands	79.37%	80.04%
Norway	63.56%	72.62%
United States	76.65%	86.42%

the mortality data. The bias-corrected intervals consistently show coverage probabilities that are closer to the nominal coverage than the bootstrapped intervals without bias-correction, indicating the effectiveness of the correction in improving the reliability of the forecast intervals. For instance, the improvement in empirical coverage is evident in Denmark, where the 95% bias-corrected interval coverage increases from 76.79% to 83.15%, and in Australia, where it rises from 83.86% to 88.48%.

However, bias-correction is not always necessary. In some cases, such as Japan, the empirical coverage probabilities are already close to the nominal levels without bias correction. For Japan, the 95% bootstrapped prediction interval coverage is 96.50%, and the bias-corrected coverage is 98.34%. This suggests that in certain contexts where the initial prediction intervals are already well-calibrated, the additional step of bias correction may not provide significant benefits.

The accuracy of the prediction intervals is closely tied to the accuracy of the point forecasts. Since bias correction centers the intervals around the point forecasts, the quality of these point forecasts directly influences the effectiveness of the interval coverage. Accurate point forecasts lead to well-centered intervals that are more likely to include the actual observed values. Conversely, if the point forecasts are biased or inaccurate, the intervals, even after bias correction, may fail to achieve the desired coverage levels. This interplay between point forecast accuracy and interval coverage will be further illustrated using the mortality data from France and Australia in Figures 11 and 12. In these plots, the black dots represent the observed mortality rates.

The prediction interval plots for France and Australia in reveal significant

differences in variability and width, reflecting the nature of each country’s mortality data. France’s data, with notable outliers due to historical events, results in wider, more conservative prediction intervals to capture greater variability. In contrast, Australia’s stable mortality rates lead to narrower intervals; however, less accurate point forecasts, particularly in the 20-40 age range, cause these intervals to miss some observed rates, especially at higher horizons.

4 Discussion

In mortality modeling and forecasting, the HUts model introduces a novel methodology by taking advantage of the universal nonlinearity of signatures and applying signature regression to decompose mortality curves. Unlike the HU model which relies on the covariance function and is sensitive to outliers, the HUts model learns data dependency through signature coefficients using principal component regression or SVD, effectively reducing the impact of outliers. The principal components obtained thus represent the structure and interactions within the data.

The HUts model has demonstrated an ability to perform competitively with, or even surpass, the other HU model variants across a different scenarios. Notably, the HUts model achieves these results without the need for weighted methods or robust statistics, which are employed by the wHU and HUrob models to improve their performance under specific conditions. This approach of the HUts model delivers robustness and is capable to adapt to diverse datasets. Whether dealing with irregularities as seen in the French mortality data or handling more stable demographic trends like those observed in Australia, the HUts model maintains high accuracy and reliability, making it a highly viable option for actuaries and demographers seeking dependable mortality forecasts without the complexity of additional methodological adjustments.

The HUts model also offers the advantage of easy modification to enhance performance, unlike the HU model’s basis expansion. Therefore, sub-optimal results are not indicative of inherent limitations but rather reflect its modular nature, allowing for greater adaptability. For instance, the embedding step is not limited to the basepoint time lead-lag transformation, Morrill et al. (2021) compiled various other augmentations that can be incorporated to improve the model. Additionally, future embeddings may better represent the geometric characteristics of a path. Besides augmentations, Morrill et al. (2021) suggested using a logsignature over the signature to reduce feature vector dimensions, and scaling paths or signatures may also offer improvements.

It is also important to acknowledge the limitations of this study. The prediction intervals constructed under the HUts model face certain limitations,

particularly due to the normality assumptions on error terms. Normality assumptions, when not justified, can lead to inaccuracies in the predicted intervals, necessitating the use of bootstrap methods. Bootstrap methods, although useful in addressing non-normality, comes more computational demand. This computational demand can be a significant drawback in practical applications where computational efficiency is crucial. In addition, bootstrap methods are sensitive to outliers which can affect the resampling process, leading to wider prediction intervals. This is evident in the case of French mortality data, which includes periods of war and disease outbreaks. These outliers introduce greater variability into the bootstrap samples, resulting in more conservative and wider intervals. This phenomenon is less pronounced in the mortality data, where the historical data is more stable and follows a general trend without significant outliers.

Future research should focus on refining the HUs model, potentially integrating more advanced smoothing techniques or exploring alternative statistical methods to enhance its performance further. Additionally, the model's application can be extended to multi-population mortality forecasting as signatures are an excellent dimension reduction tool and incorporating socioeconomic factors as a binary dimension could provide deeper insights into mortality trends. The following practical extensions can be readily implemented:

1. Gender specific HUs model

$$\begin{aligned} \text{Male: } f_{t,M}(x) &= \mu(x) + \sum_{k=1}^K \beta_{t,k} Z_k(x) + e_t(x), \\ \text{Female: } f_{t,F}(x) &= \mu(x) + \sum_{k=1}^K \beta_{t,k} Z_k(x) + e_t(x). \end{aligned}$$

This adaptation allows the model to capture and forecast mortality trends separately for different genders, taking into account potential differences in mortality patterns, improvements, and other gender-specific characteristics.

2. Fitting the HUs model with mortality improvement rates, $z_{x,t} = 2 \times \frac{1 - \frac{m_{x,t}}{m_{x,t-1}}}{1 + \frac{m_{x,t}}{m_{x,t-1}}}$ instead of raw mortality rates $m_{x,t}$ (Haberman and Renshaw, 2012). Let the underlying smoothed function of $z_{x,t}$ be $\gamma_t(x)$, then using the HUs we can decompose it into:

$$\gamma_t(x) = \mu(x) + \sum_{k=1}^K \beta_{t,k} Z_k(x) + e_t(x).$$

Modeling mortality improvement rates helps stabilize the mortality data series by focusing on changes over time, making it stationary and enhancing the accuracy of forecasts.

3. Coherent mortality forecasting using the product ratio method by Hyndman et al. (2012) by fitting $p_t(x) = \sqrt{f_{t,M}(x) \cdot f_{t,F}(x)}$ and $r_t(x) = \sqrt{\frac{f_{t,M}(x)}{f_{t,F}(x)}}$ using the HUts model and forecasting it h -steps-ahead. Then the h -steps-ahead forecasts of the gender specific log mortality rates can be obtained as follows:

$$\begin{aligned} f_{n+h|n,M}(x) &= p_{n+h|n}(x) \times r_{n+h|n}(x), \\ f_{n+h|n,F}(x) &= \frac{p_{n+h|n}(x)}{r_{n+h|n}(x)}. \end{aligned}$$

This method ensures that the mortality forecasts for different subpopulations remain within realistic and historically observed relationships. Jiménez-Varón et al. (2024); Shang et al. (2022); Shang and Hyndman (2017) also provide potential directions for extending the HUts model for subpopulation modelling.

In addition, the performance of the HUts model, like any other model, depends on the country's data and forecast horizon, with some models performing relatively better in certain settings. This emphasizes the influence of country-specific mortality dynamics and model sensitivities. As Shang (2012) pointed out, there is no universal mortality model capable of effectively handling data from all countries. This makes the HUts model a candidate for model averaging approaches. Model averaging combines the strengths of various models to improve forecast accuracy by assigning empirical weights to each model based on their performance at different horizons. Given the HUts model's demonstrated efficacy, especially in long-term forecasts, it can be assigned greater weight in model-averaged forecasts to leverage its strengths (Shang and Booth, 2020). The benefits of model averaging lie in enhancing forecast accuracy through a strategic combination of models. By integrating the HUts model into a model averaging framework, it is possible to achieve more reliable and accurate mortality forecasts, particularly over longer forecast horizons.

Beyond demography, the HUts model extends itself offering a robust framework for addressing a range of challenges in functional data analysis, including functional principal component regression (FPCR), functional regression with functional responses, and forecasting functional time series. The flexibility of the HUts model to adapt to various functional data analysis scenarios is primarily due to its ability to integrate advanced mathematical concepts from functional data analysis, such as smoothing, handling of high-dimensional datasets. This integration not only enhances the model's

performance in demographic forecasting but also makes it a powerful tool for broader applications in statistical and machine learning fields involving complex, structured data.

5 Conclusion

This paper has introduced the incorporation of signatures into the HU model, resulting in the HUts model. It not only outperforms the HU model but also exhibits enhanced robustness, particularly in the presence of outliers and irregularities in the data. The empirical results from the French and other mortality datasets provide compelling evidence of the HUts model's efficacy. In the case of France, with the presence of notable historical outliers due to wars and disease outbreaks, the HUts model showed substantial improvement over the HU model. This is evident from the lower MSE and MAE values across various forecast horizons. The enhanced performance can be attributed to the model's ability to mitigate the influence of outliers, which are more prevalent in the French data. This robustness is crucial for accurate mortality forecasting in regions with volatile historical trends. The HUts model's superior performance across all age groups, particularly at longer forecast horizons, underscores its utility even in more stable datasets. This consistency across diverse demographic conditions highlights the model's versatility and reliability. Prediction intervals were constructed with the application of bootstrap procedures. The coverage probabilities of the 80% and 95% bootstrapped prediction intervals with and without bias correction reveal that bias-corrected intervals generally provide better coverage, especially in the absence of outliers. This is particularly pronounced in the French data, where the intervals constructed were more conservative and wide. In contrast, the Australian data, with fewer outliers, shows smaller coverage deviance with its bias corrected bootstrapped prediction interval. From a practical standpoint, these findings have significant implications for actuaries and policymakers. The improved accuracy and robustness of the HUts model can lead to more reliable mortality forecasts, which are essential for various applications, including insurance pricing, pension fund management, and public health planning. The model's ability to handle data with outliers and provide accurate long-term forecasts makes it a valuable tool for demography.

A Appendix

A.1 Normality assumptions of errors

To obtain prediction intervals using distributional forecasts, all sources of error must satisfy the normality assumptions. If any source of error does not

follow a normal distribution, bootstrapping methods should be used instead. The model residual histograms of ages 0, 25, 40 and 70 of the HUTs model fitted with French mortality data are plotted with a superimposed normal distribution curve are in Figure 13. It is evident that the residuals do not conform to a normal distribution.

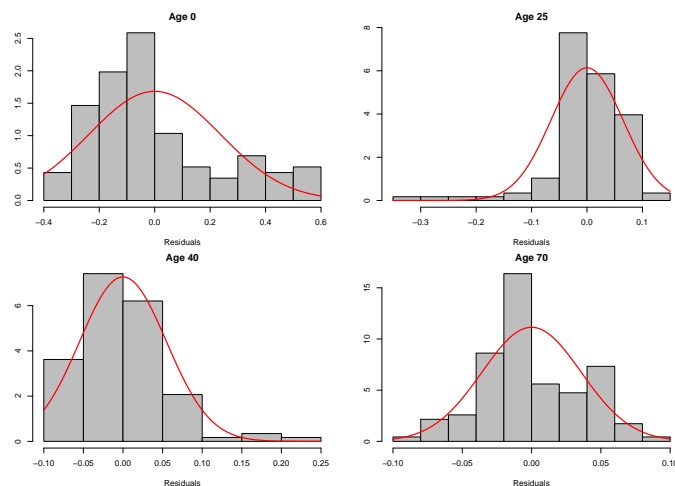


Figure 13: Residual histograms of ages 0, 25, 40 and 70

A.2 Selection of truncation order

As the number of signature coefficients increases exponentially with the truncation order, we employ a naive search based on the MSE and MAE of the model's forecasting performance. In signature regression, it is generally advisable to keep the truncation order, m , below 5. A truncation order of 5 already includes 182 signature coefficients, significantly impacting the computational effort required. This approach is demonstrated using French mortality data. As depicted in Figure 14, the MSE and MAE values of the HUTs model with $m = 3, 4, 5$ are larger than when $m = 2$. Since our path dimension is only 3, a high order of signature coefficients may not be necessary to accurately represent the path.

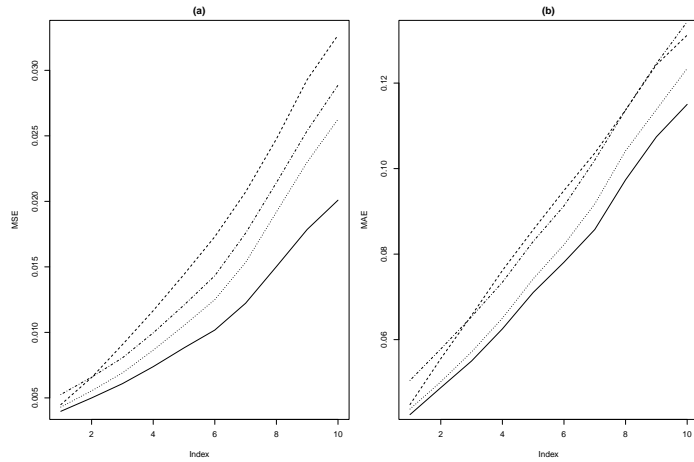


Figure 14: (a) MSE and (b) MAE plots for French mortality of the HUts model with $m = 2$ (solid line), $m = 3$ (dashed line), $m = 4$ (dotted line), and $m = 5$ (dash-dotted line)

A.3 Remaining MSE and MAE plots

In this section, we categorized the MSE and MAE plots of the remaining 10 countries into two groups: those favorable to the HUts model and those where the HUts model is comparable to the other models.

A.3.1 Favourable to the HUts model

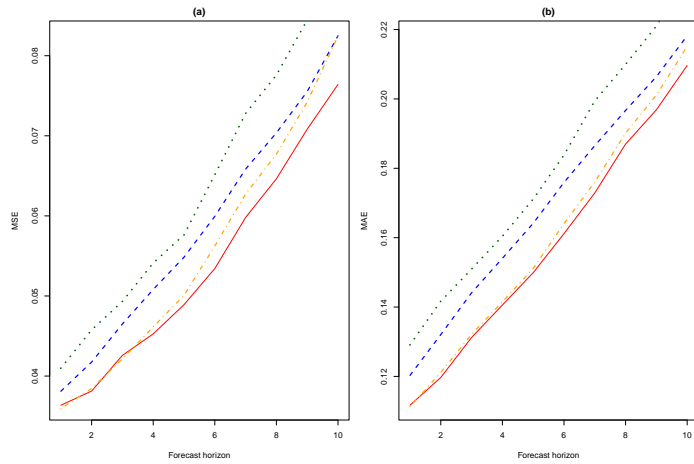


Figure 15: (a) MSE and (b) MAE plots for Danish mortality of the HUts (red solid line), HU (blue dashed line), HUrob (green dotted line), and the wHU (orange dash-dotted line) models

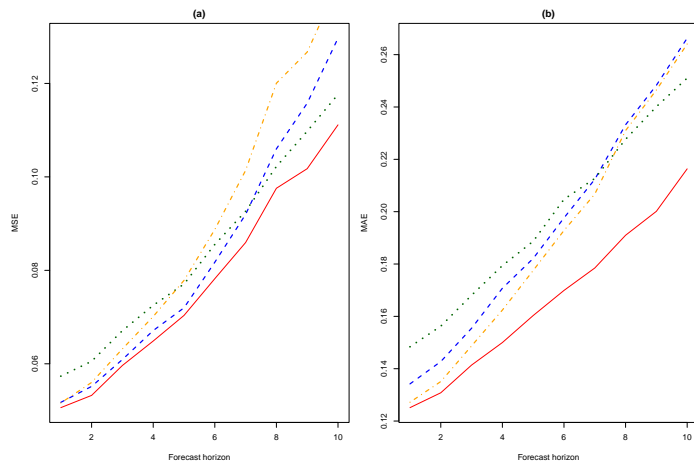


Figure 16: (a) MSE and (b) MAE plots for Irish mortality of the HUts (red solid line), HU (blue dashed line), HUrob (green dotted line), and the wHU (orange dash-dotted line) models

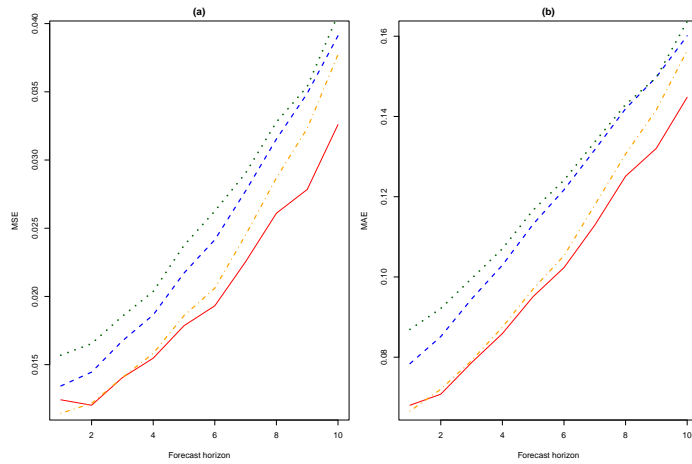


Figure 17: (a) MSE and (b) MAE plots for Dutch mortality of the HUs (red solid line), HU (blue dashed line), HUrob (green dotted line), and the wHU (orange dash-dotted line) models

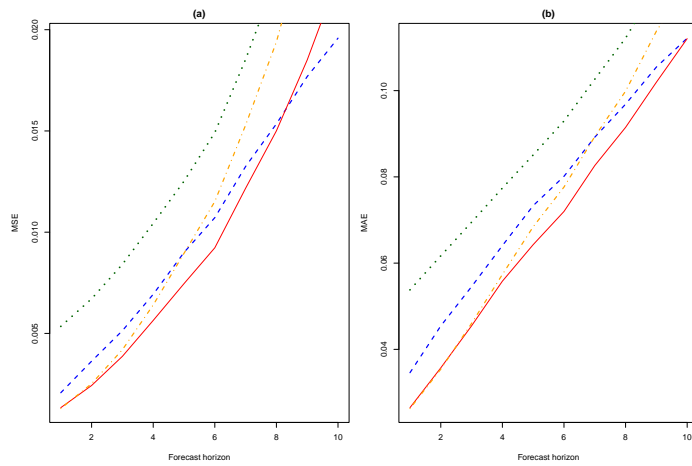


Figure 18: (a) MSE and (b) MAE plots for American mortality of the HUs (red solid line), HU (blue dashed line), HUrob (green dotted line), and the wHU (orange dash-dotted line) models

A.3.2 Comparable to the HUts model

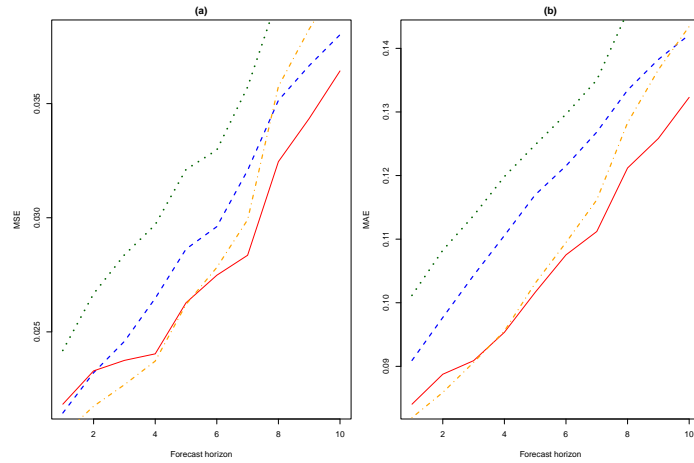


Figure 19: (a) MSE and (b) MAE plots for Belgian mortality of the HUts (red solid line), HU (blue dashed line), HUrob (green dotted line), and the wHU (orange dash-dotted line) models

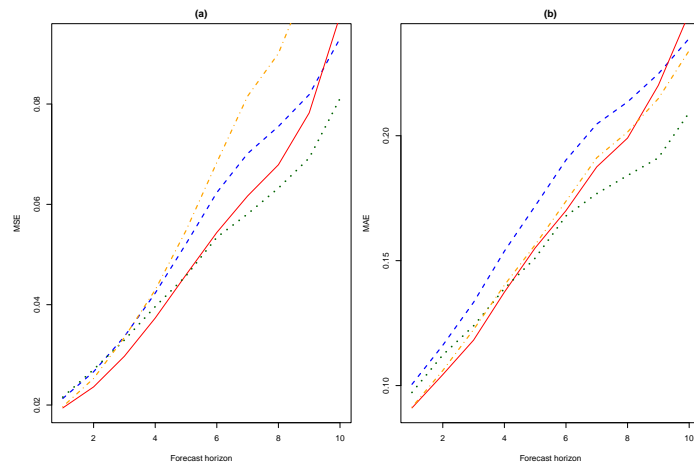


Figure 20: (a) MSE and (b) MAE plots for Bulgarian mortality of the HUts (red solid line), HU (blue dashed line), HUrob (green dotted line), and the wHU (orange dash-dotted line) models

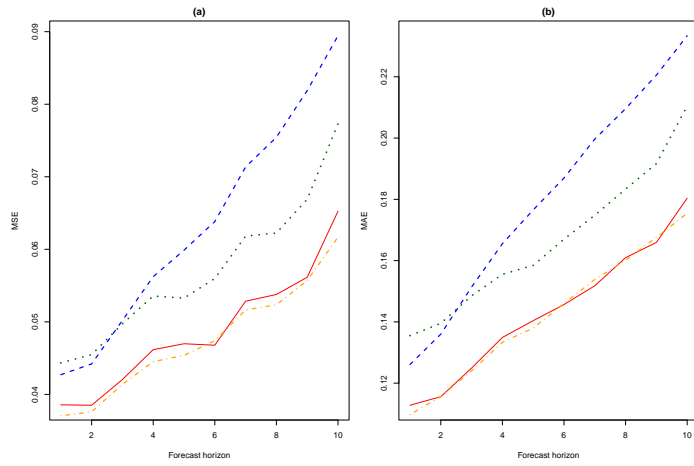


Figure 21: (a) MSE and (b) MAE plots for Finnish mortality of the HUs (red solid line), HU (blue dashed line), HUrob (green dotted line), and the wHU (orange dash-dotted line) models

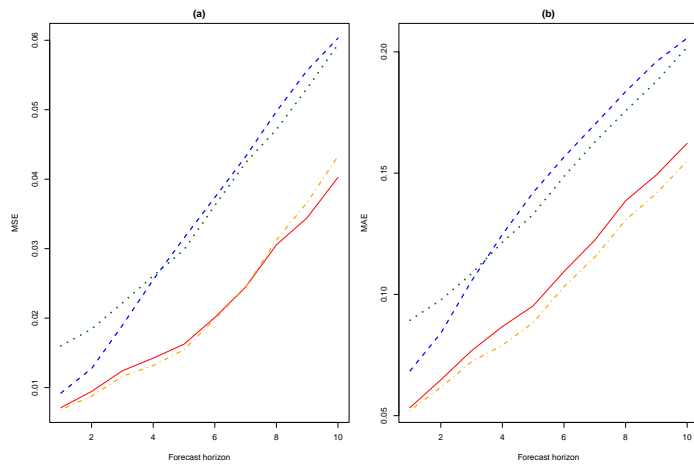


Figure 22: (a) MSE and (b) MAE plots for Italian mortality of the HUs (red solid line), HU (blue dashed line), HUrob (green dotted line), and the wHU (orange dash-dotted line) models

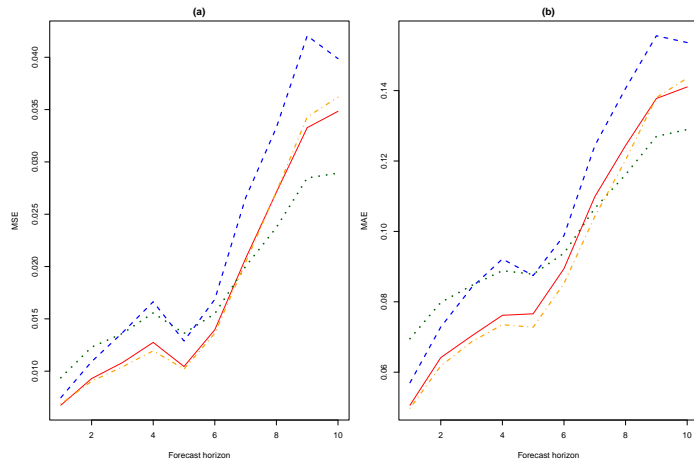


Figure 23: (a) MSE and (b) MAE plots for Japanese mortality of the HUs (red solid line), HU (blue dashed line), HUrob (green dotted line), and the wHU (orange dash-dotted line) models

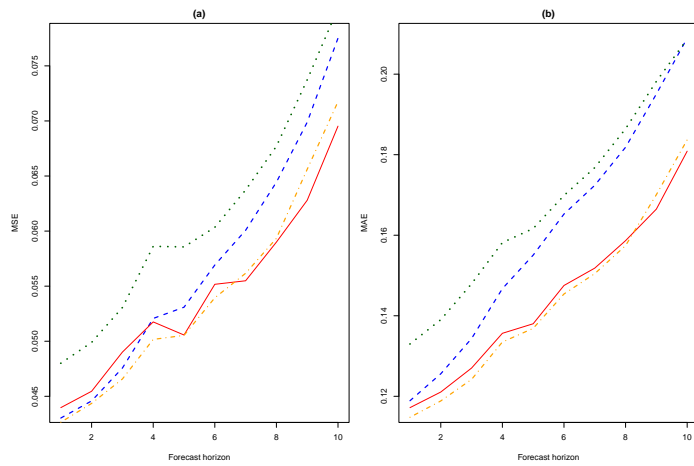


Figure 24: (a) MSE and (b) MAE plots for Norwegian mortality of the HUs (red solid line), HU (blue dashed line), HUrob (green dotted line), and the wHU (orange dash-dotted line) models

References

- Hervé Andrès, Alexandre Boumezoued, and Benjamin Jourdain. Signature-based validation of real-world economic scenarios. *ASTIN Bulletin*, 54(2): 410–440, 2024. doi: 10.1017/asb.2024.12.
- Ugofilippo Basellini, Carlo Giovanni Camarda, and Heather Booth. Thirty years on: A review of the lee–carter method for forecasting mortality. *International Journal of Forecasting*, 39(3):1033–1049, 2023. ISSN 0169-2070. doi: 10.1016/j.ijforecast.2022.11.002.
- Dorethe Skovgaard Bjerre. Tree-based machine learning methods for modeling and forecasting mortality. *ASTIN Bulletin*, 52(3):765–787, 2022. doi: 10.1017/asb.2022.11.
- Patric Bonnier, Patrick Kidger, Imanol Perez Arribas, Cristopher Salvi, and Terry Lyons. Deep signature transforms, 2019.
- H. Booth and L. Tickle. Mortality modelling and forecasting: a review of methods. *Annals of Actuarial Science*, 3(1–2):3–43, 2008. doi: 10.1017/S1748499500000440.
- Heather Booth, John Maindonald, and Len Smith. Applying lee-carter under conditions of variable mortality decline. *Population Studies*, 56(3):325–336, 2002. ISSN 00324728. doi: 10.1080/00324720215935.
- Chris Chatfield. Calculating interval forecasts. *Journal of Business & Economic Statistics*, 11(2):121–135, 1993. ISSN 07350015. doi: 10.2307/1391361.
- Chung Chen and Lon-Mu Liu. Joint estimation of model parameters and outlier effects in time series. *Journal of the American Statistical Association*, 88(421):284–297, 1993. ISSN 01621459. doi: 10.2307/2290724.
- Kuo-Tsai Chen. Integration of paths, geometric invariants and a generalized baker-hausdorff formula. *Annals of Mathematics*, 65(1):163–178, 1957. ISSN 0003486X. doi: 10.2307/1969671.
- Samuel N. Cohen, Silvia Lui, Will Malpass, Giulia Mantoan, Lars Nesheim, Álvaro de Paula, Andrew Reeves, Craig Scott, Emma Small, and Lingyi Yang. Nowcasting with signature methods, 2023.
- Claudia Czado, Antoine Delwarde, and Michel Denuit. Bayesian poisson log-bilinear mortality projections. *Insurance: Mathematics and Economics*, 36(3):260–284, 2005. ISSN 0167-6687. doi: 10.1016/j.insmatheco.2005.01.001.

- Philippe Deprez, Pavel Shevchenko, and Mario Wüthrich. Machine learning techniques for mortality modeling. *European Actuarial Journal*, 7: 337–352, 2017. doi: 10.1007/s13385-017-0152-4.
- Alexander Dokumentov, Rob J. Hyndman, and Leonie Tickle. Bivariate smoothing of mortality surfaces with cohort and period ridges. *Stat*, 7(1): e199, 2018. doi: 10.1002/sta4.199.
- Bradley Efron and Robert J. Tibshirani. *An Introduction to the Bootstrap*. Number 57 in Monographs on Statistics and Applied Probability. Chapman & Hall/CRC, Boca Raton, Florida, USA, 1993.
- Adeline Fermanian. Embedding and learning with signatures. *Computational Statistics & Data Analysis*, 157:107148, 2021. ISSN 0167-9473. doi: 10.1016/j.csda.2020.107148.
- Adeline Fermanian. Functional linear regression with truncated signatures. *Journal of Multivariate Analysis*, 192:105031, 2022. ISSN 0047-259X. doi: 10.1016/j.jmva.2022.105031.
- Camille Frévent. A functional spatial autoregressive model using signatures, 2023.
- Steven Haberman and Arthur Renshaw. Parametric mortality improvement rate modelling and projecting. *Insurance: Mathematics and Economics*, 50(3):309–333, 2012. ISSN 0167-6687. doi: 10.1016/j.insmatheco.2011.11.005.
- Ben Hambly and Terry Lyons. Uniqueness for the signature of a path of bounded variation and the reduced path group. *Annals of Mathematics*, pages 109–167, 2010. URL <https://www.jstor.org/stable/27799199>.
- Mia Hubert, Peter J. Rousseeuw, and Sabine Verboven. A fast method for robust principal components with applications to chemometrics. *Chemometrics and Intelligent Laboratory Systems*, 60(1):101–111, 2002. ISSN 0169-7439. doi: [https://doi.org/10.1016/S0169-7439\(01\)00188-5](https://doi.org/10.1016/S0169-7439(01)00188-5).
- Human Mortality Database, 2024. URL www.mortality.org.
- Rob J. Hyndman and Heather Booth. Stochastic population forecasts using functional data models for mortality, fertility and migration. *International Journal of Forecasting*, 24(3):323–342, 2008. ISSN 0169-2070. doi: 10.1016/j.ijforecast.2008.02.009.
- Rob J. Hyndman and Han Lin Shang. Forecasting functional time series. *Journal of the Korean Statistical Society*, 38(3):199–211, 2009. ISSN 1226-3192. doi: 10.1016/j.jkss.2009.06.002.

- Rob J. Hyndman and Md. Shahid Ullah. Robust forecasting of mortality and fertility rates: A functional data approach. *Computational Statistics & Data Analysis*, 51(10):4942–4956, 2007. ISSN 0167-9473. doi: 10.1016/j.csda.2006.07.028.
- Rob J. Hyndman, Heather Booth, and Farah Yasmeen. Coherent Mortality Forecasting: The Product-Ratio Method With Functional Time Series Models. *Demography*, 50(1):261–283, 10 2012. doi: 10.1007/s13524-012-0145-5.
- Cristian F. Jiménez-Varón, Ying Sun, and Han Lin Shang. Forecasting high-dimensional functional time series: Application to sub-national age-specific mortality. *Journal of Computational and Graphical Statistics*, 0(0):1–15, 2024. doi: 10.1080/10618600.2024.2319166.
- Jasdeep Kalsi, Terry Lyons, and Imanol Perez Arribas. Optimal execution with rough path signatures. *SIAM Journal on Financial Mathematics*, 11(2):470–493, 2020. doi: 10.1137/19M1259778.
- Patrick Kidger and Terry Lyons. Universal approximation with deep narrow networks. In Jacob Abernethy and Shivani Agarwal, editors, *Proceedings of Thirty Third Conference on Learning Theory*, volume 125 of *Proceedings of Machine Learning Research*, pages 2306–2327. PMLR, 2020. URL <https://proceedings.mlr.press/v125/kidger20a.html>.
- Franz J. Kiraly and Harald Oberhauser. Kernels for sequentially ordered data. *Journal of Machine Learning Research*, 20(31):1–45, 2019. URL <http://jmlr.org/papers/v20/16-314.html>.
- Ronald D. Lee and Lawrence R. Carter. Modeling and forecasting u. s. mortality. *Journal of the American Statistical Association*, 87(419):659–671, 1992. ISSN 01621459. doi: 10.2307/2290201.
- Ronald D. Lee and Timothy Miller. Evaluating the performance of the lee-carter method for forecasting mortality. *Demography*, 38(4):537–549, 2001. ISSN 00703370, 15337790. doi: 10.2307/3088317.
- Daniel Levin, Terry Lyons, and Hao Ni. Learning from the past, predicting the statistics for the future, learning an evolving system, 2016.
- Terry Lyons, Michael Caruana, and Thierry Lévy. *Differential Equations Driven by Moderately Irregular Signals*, pages 1–24. Springer Berlin Heidelberg, Berlin, Heidelberg, 2007. ISBN 978-3-540-71285-5. doi: 10.1007/978-3-540-71285-5_1. URL https://doi.org/10.1007/978-3-540-71285-5_1.

- Terry Lyons, Sina Nejad, and Imanol Perez Arribas. Non-parametric pricing and hedging of exotic derivatives. *Applied Mathematical Finance*, 27(6): 457–494, 2020. doi: 10.1080/1350486X.2021.1891555.
- James Morrill, Andrey Kormilitzin, Alejo J. Nevado-Holgado, Sumanth Swaminathan, Samuel D. Howison, and Terry J. Lyons. Utilization of the signature method to identify the early onset of sepsis from multivariate physiological time series in critical care monitoring. *Critical Care Medicine*, 48(10), 2020. ISSN 0090=3493. doi: 10.1097/CCM.0000000000004510. URL https://journals.lww.com/ccmjournal/fulltext/2020/10000/utilization_of_the_signature_method_to_identify.43.aspx.
- James Morrill, Adeline Fermanian, Patrick Kidger, and Terry Lyons. A generalised signature method for multivariate time series feature extraction, 2021.
- J. O. Ramsay and B. W. Silverman. *Functional Data Analysis*. Springer, 2005. ISBN 9780387400808. URL <http://www.worldcat.org/isbn/9780387400808>.
- Arthur Renshaw and Steven Haberman. Lee-carter mortality forecasting: A parallel generalized linear modelling approach for england and wales mortality projections. *Journal of the Royal Statistical Society. Series C (Applied Statistics)*, 52(1):119–137, 2003. ISSN 00359254, 14679876. URL <http://www.jstor.org/stable/3592636>.
- Han Lin Shang. Point and interval forecasts of age-specific life expectancies: A model averaging approach. *Demographic Research*, 27(21): 593–644, 2012. doi: 10.4054/DemRes.2012.27.21. URL <https://www.demographic-research.org/volumes/vol27/21/>.
- Han Lin Shang and Heather Booth. Synergy in fertility forecasting: improving forecast accuracy through model averaging. *Genus*, 76(1):27, 9 2020. ISSN 2035-5556. doi: 10.1186/s41118-020-00099-y. URL <https://doi.org/10.1186/s41118-020-00099-y>.
- Han Lin Shang and Rob J. Hyndman. Grouped functional time series forecasting: An application to age-specific mortality rates. *Journal of Computational and Graphical Statistics*, 26(2):330–343, 2017. doi: 10.1080/10618600.2016.1237877.
- Han Lin Shang, Steven Haberman, and Ruofan Xu. Multi-population modelling and forecasting life-table death counts. *Insurance: Mathematics and Economics*, 106:239–253, 2022. ISSN 0167-6687. doi: 10.1016/j.insmatheco.2022.07.002. URL <https://www.sciencedirect.com/science/article/pii/S0167668722000750>.

Bo Wang, Yue Wu, Niall Taylor, Terry Lyons, Maria Liakata, Alejo J. Nevado-Holgado, and Kate E.A. Saunders. Learning to Detect Bipolar Disorder and Borderline Personality Disorder with Language and Speech in Non-Clinical Interviews. In *Proc. Interspeech 2020*, pages 437–441, 2020. doi: 10.21437/Interspeech.2020-3040.

Zecheng Xie, Zenghui Sun, Lianwen Jin, Hao Ni, and Terry Lyons. Learning spatial-semantic context with fully convolutional recurrent network for online handwritten chinese text recognition. *IEEE Transactions on Pattern Analysis and Machine Intelligence*, 40(8):1903–1917, 2018. doi: 10.1109/TPAMI.2017.2732978.